Computation of frictional multi-contact equilibrium stances and postures on 3D uneven tame terrains

Yizhar Or*and Elon Rimon

Technical Report, Dept. of Mechanical Engineering, Technion, Israel

December 1, 2014

1 Preliminaries and Problem Statement

This section defines the terminology and notation used throughout the paper, and then formulates the problem analyzed in this paper. Let a 3D object $\mathcal{B}$ be supported by n frictional point contacts, whose position vectors are given by $\boldsymbol{x}_1 \dots \boldsymbol{x}_n \in I\!R^3$. We use the standard basis to $I\!R^3$ such that $\boldsymbol{e} = (0\ 0\ 1)^T$ is the upward vertical direction. Let $\boldsymbol{x}_c$ denote the position of $\mathcal{B}$'s center-of-mass, and let $\boldsymbol{f}_g$ denote the gravitational force acting at $\boldsymbol{x}_c$. Let $\boldsymbol{f}_1 \dots \boldsymbol{f}_n \in I\!R^3$ be the contact reaction forces. We assume *hard-finger contacts* which generate negligible torque about the contact normals. Finally, we denote the matrix $\mathbf{E} = \begin{pmatrix} 1 & 0 & 0 \\ 0 & 1 & 0 \end{pmatrix}$ which projects a vector in $I\!R^3$ onto the horizontal plane. The horizontal projections of contact points, contact forces, and center-of-mass position are deonted by $\tilde{\boldsymbol{x}}_i = \mathbf{E}\boldsymbol{x}_i$, $\tilde{\boldsymbol{f}}_i = \mathbf{E}\boldsymbol{f}_i$ and $\tilde{\boldsymbol{x}}_c = \mathbf{E}\boldsymbol{x}_c$, respectively.

The static equilibrium condition for a given n-contact arrangement is given by

$$\sum_{i=1}^{n} \begin{pmatrix} \boldsymbol{f}_i \\ \boldsymbol{x}_i \times \boldsymbol{f}_i \end{pmatrix} = - \begin{pmatrix} \boldsymbol{f}_g \\ \boldsymbol{x}_c \times \boldsymbol{f}_g \end{pmatrix}. \tag{1}$$

For a given arrangement of $n \geq 3$ contacts and center-of-mass position $\boldsymbol{x}_c$, the static balance condition (1) is indeterminate, and the solution for $\boldsymbol{f}_1 \dots \boldsymbol{f}_n$ is generically a $(3n-6)$-dimensional affine space in $I\!R^{3n}$. Under Coulomb's friction model the contact forces must additionally lie in their respective *friction cones*. The i^{th} friction cone is denoted C_i and is given by

$$C_i = \{\boldsymbol{f}_i : ||\boldsymbol{f}_i - (\boldsymbol{f}_i \cdot \boldsymbol{n}_i)\boldsymbol{n}_i|| \leq \mu_i(\boldsymbol{f}_i \cdot \boldsymbol{n}_i)\}, \tag{2}$$

where μ_i is Coulomb's coefficient of static friction at the i^{th} contact and $\boldsymbol{n}_i$ is the outward unit normal at x_i. The physical meaning of (2) is that the magnitude of the tangential component of the contact force $\boldsymbol{f}_i$ must be less than or equal to μ_i times the magnitude of the normal contact force $\boldsymbol{f}_i \cdot \boldsymbol{n}_i$. Throughout the paper, we will often embed the friction

*Corresponding author: Dept. of ME, Technion, Haifa, Israel 32000, izi@tx.technion.ac.il.

cones in the physical space by shifting the origin of each cone C_i to the contact point $\boldsymbol{x}_i$ as in Fig. 1(a). These physical friction cones depict the feasible lines of action of the contact forces $\boldsymbol{f}_i$. Assuming that the contacts points and their respective friction cones are given, the feasible equilibrium region of center-of-mass locations is defined as follows.

Definition 1. *For a given arrangement of contacts* $\{\boldsymbol{x}_1 \dots \boldsymbol{x}_n\}$*, contact normals* $\{\boldsymbol{n}_1 \dots \boldsymbol{n}_n\}$*, and coefficients of static friction* $\{\mu_1 \dots \mu_n\}$*, the* **feasible equilibrium region***, denoted* $\mathcal{R}$*, is the region of all possible center-of-mass locations* $\boldsymbol{x}_c$ *for which there exist contact reaction forces* $\boldsymbol{f}_i \in C_i$ *(*$i = 1 \dots n$*) satisfying the static equilibrium condition (1).*

The goal of this paper is to extend the results of our previous work which characterized the feasible equilibrium region $\mathcal{R}$ for $n = 3$ contacts to the general case of $n > 3$ contacts.

2 Basic properties of the equilibrium region

In this section, we review some basic properties of the feasible equilibrium region $\mathcal{R}$, which were proven in our previous paper [IJRR 2010]. Then we generalize the notion of tame contact arrangement to the case of $n > 3$ and discuss its relation to the support polygon principle. The first observations on basic properties of $\mathcal{R}$ are summarized in the following proposition.

Proposition 2.1. *Let a 3D object* $\mathcal{B}$ *be supported by n frictional contacts against gravity in three-dimensions. If the feasible equilibrium region* $\mathcal{R}$ *is nonempty, it is a vertical line for a single contact, a vertical strip for two contacts, and generically a three-dimensional* **right cylinder with convex cross-section** *for* $n \geq 3$ *contacts.*

It is worth noting that for a single contact $\mathcal{R}$ is a vertical line passing through the contact, and for two contacts it is a vertical strip in the plane passing through the contacts. For $n \geq 3$ contacts, a special case occurs when all contacts are aligned along a common spatial line. In this non-generic case $\mathcal{R}$ degenerates to a two-dimensional vertical strip embedded in the vertical plane passing through the contacts. Based on the proposition, the computation of $\mathcal{R}$ requires computation of its *horizontal cross-section*, denoted $\widetilde{\mathcal{R}}$, in $I\!R^2$. From this point and on, we will refer to the cross-section $\widetilde{\mathcal{R}} \subset I\!R^2$ as the equilibrium region.

Tame contact arrangements and the support polygon: When computing equilibrium postures on a flat horizontal terrain, a classical concept is the **support polygon principle**, which states that the center-of-mass must lie above the polygon spanned by the contacts. Formally, the support polygon $\Pi \subset I\!R^2$ is defined as the polygonal region spanned by the horizontal projection of all contact points, namely, $\Pi = \text{conv}\{\tilde{\boldsymbol{x}}_1 \dots \tilde{\boldsymbol{x}}_n\}$. It can be readily shown that on a flat horizontal terrain with n frictional contacts (i.e. $\boldsymbol{n}_i = \boldsymbol{e}$ and $\boldsymbol{e} \cdot \boldsymbol{x}_i = h = \text{const}$ for $i = 1 \dots n$), the equilibrium region $\widetilde{\mathcal{R}}$ is precisely equal to Π. However, if the terrain is not flat, the relation between $\widetilde{\mathcal{R}}$ and the support polygon Π can be more involved. In the previous paper, we have introduced a subclass of 3-contact arrangements called *tame*, for which $\widetilde{\mathcal{R}}$ is fully contained in Π. In the following, we extend the notion of tame contact arrangements to n contacts. First, denote by $\partial\Pi$ the boundary of the support polygon, which is a collection of line segments connecting pairs of projected contacts $(\tilde{\boldsymbol{x}}_i, \tilde{\boldsymbol{x}}_j)$ which form a closed loop. Note that not all the contact points necessarily contribute to $\partial\Pi$. The generalized definition of tame contact arrangement is then given as follows.

Definition 2. *A contact arrangement of n frictional contacts is called* **tame** *if each line segment* $(\tilde{\boldsymbol{x}}_i, \tilde{\boldsymbol{x}}_j) \in \partial\Pi$ *satisfies*

$$\mathrm{sgn}((\boldsymbol{x}_i - \boldsymbol{x}_j) \cdot (\boldsymbol{x}_k - \boldsymbol{x}_i) \times \boldsymbol{f}_k) = \mathrm{sgn}((\boldsymbol{x}_i - \boldsymbol{x}_j) \cdot (\boldsymbol{x}_k - \boldsymbol{x}_i) \times \boldsymbol{e})$$

for all $\boldsymbol{f}_k \in C_k$ *and all* $k \in \{1 \dots n\} \setminus \{i, j\}$.

Geometrically, the definition means that each friction cone C_k emanating from the contact point $\boldsymbol{x}_k$ for $k \neq i, j$ lies entirely above the line segment $(\tilde{\boldsymbol{x}}_i, \tilde{\boldsymbol{x}}_j)$. Note that for $n = 3$ contacts, this definition of tame reduces to the one given in our previous paper.

Next, we recall the definition of a quasi-flat contact. A contact $\boldsymbol{x}_i$ whose corresponding friction cone is given by C_i is called **quasi-flat** if $\boldsymbol{e} \in C_i$, where $\boldsymbol{e}$ is the upward vertical direction. It is clear that a quasi-flat contact $\boldsymbol{x}_i$ satisfies $\tilde{\boldsymbol{x}}_i \in \widetilde{\mathcal{R}}$, since a contact force $\boldsymbol{f}_i = \boldsymbol{e}$ balances the net forces and torques when $\boldsymbol{x}_c$ lies above $\boldsymbol{x}_i$, while all other contact forces are zero. The following proposition summarizes the relations between $\widetilde{\mathcal{R}}$ and Π.

Proposition 2.2. *For a* **tame** *n-contact arrangement, the equilibrium region* $\widetilde{\mathcal{R}}$ *is fully contained in the support polygon,* $\widetilde{\mathcal{R}} \subseteq \Pi$. *The converse relationship,* $\Pi \subseteq \widetilde{\mathcal{R}}$, *always holds when all contacts are* **quasi-flat**.

The proposition implies that for tame contact arrangements such that all contacts are quasi-flat one obtains $\widetilde{\mathcal{R}} = \Pi$. This equality holds for a flat horizontal terrain with or without friction, and also persists under small variations in the contact arrangements, which verifies the validity of the support polygon principle on terrains which are nearly flat. In this paper, we restrict ourselves to tame contact arrangements, for which $\widetilde{\mathcal{R}}$ is fully contained in the support polygon Π. Nevertheless, if some contacts that lie on $\partial\Pi$ are not quasi-flat, as commonly occurs in scenarios of uneven terrain, one obtains that $\widetilde{\mathcal{R}} \subset \Pi$, and the support polygon principle is no longer a safe criterion for finding equilibrium postures. In such cases, one has to explicitly compute the feasible equilibrium region, whose boundary can be much more complicated than a simple polygon. This computation is the main contribution of our paper.

Graphical examples: We now illustrate the application of Proposition 2.2 to two contact arrangements, and emphasize the dependence on friction coefficients. Figure 1(a) shows an arrangement of four contacts with uniform friction coefficient μ on a step. All contacts lie on horizontal surfaces, i.e. $\boldsymbol{n}_i = \boldsymbol{e}$ for $i = 1, 2, 3, 4$ so that all contacts are quasi-flat, which implies that $\widetilde{\mathcal{R}} \subseteq \Pi$. The vertical height of the step is l and the horizontal distance between the contacts on the lower step and the contacts on the lower step is h. Using definition 2, it can be verified that the contact arrangement is tame if and only if the coefficient of friction satisfies $\mu < l/h$. According to Proposition 2.2, when this condition is satisfied the equilibrium region satisfies $\widetilde{\mathcal{R}} = \Pi$. When the friction is large or the vertical height of the step is increased, this condition is violated, so that the equilibrium region satisfies $\widetilde{\mathcal{R}} \supset \Pi$.

Figure 1(b) shows an arrangement of five contacts. Each contact normal makes an angle of 30° with the vertical direction $\boldsymbol{e}$, and the coefficient of friction μ is equal at all contacts. The physical friction cone C_3 appears in the Figure for $\mu = 0.8$. In this case, it can be seen that the friction cone C_3 intersects the line $\boldsymbol{x}_1 - \boldsymbol{x}_5$, so that the contact arrangement is not tame. On the other hand, all contacts are quasi-flat, hence the feasible equilibrium region satisfies $\widetilde{\mathcal{R}} \supset \Pi$. For $\mu = 0.7$, the contact arrangement becomes tame,

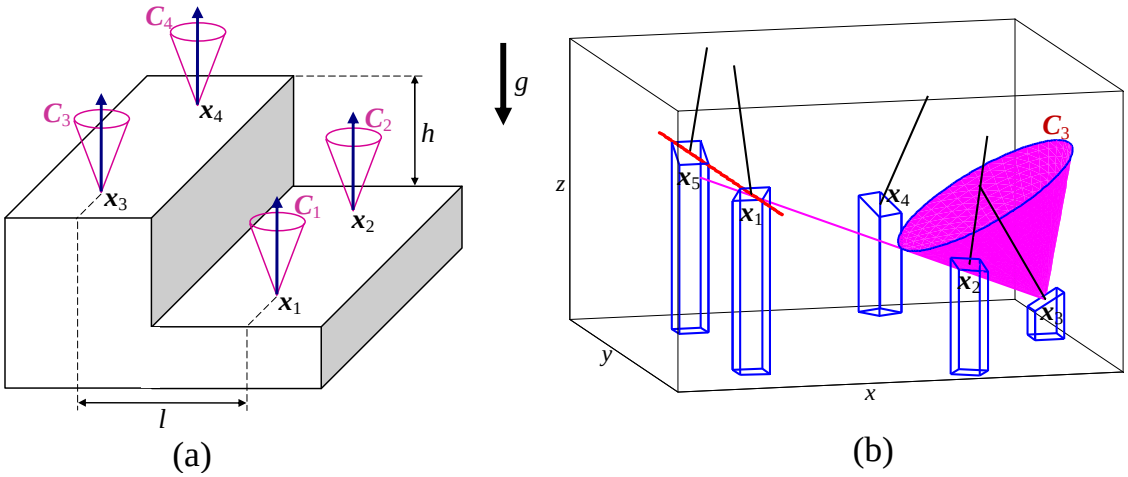

Figure 1: Examples of non-tame contact arrangements

while all contacts remains quasi-flat, hence the feasible equilibrium region satisfies $\widetilde{\mathcal{R}} = \Pi$. For $\mu < 1/\sqrt{3} \approx 0.577$, the arrangement is tame but all contacts are no longer quasi-flat (i.e. $\boldsymbol{e} \notin C_i$) and the feasible equilibrium region lies strictly inside the support polygon, i.e. $\widetilde{\mathcal{R}} \subset \Pi$.

3 Exact computation of the equilibrium region

This section presents the main result of the paper — exact computation of the equilibrium region $\widetilde{\mathcal{R}}$ and geometric characterization of its boundary. The basis of this computation is a geometric interpretation of the static equilibrium equation (1). This equation lives in the six-dimensional *wrench space* of forces and torques. The left hand side of (1) represents the net wrench generated by the contact forces $\boldsymbol{f}_1 \dots \boldsymbol{f}_n$. Each contact force $\boldsymbol{f}_i$ is restricted to lie within its (convex) friction cone C_i, defined in (2). Thus, the net wrench generated by the contact forces spans a six-dimensional convex cone W in $\mathbb{R}^6$, which is defined as

$$W = \left\{ \sum_{i=1}^{n} \begin{pmatrix} \boldsymbol{f}_i \\ \boldsymbol{x}_i \times \boldsymbol{f}_i \end{pmatrix} \text{ for all } \boldsymbol{f}_i \in C_i, \;\; i = 1 \dots n \right\}. \tag{3}$$

As the horizontal projection of the center-of-mass $\tilde{\boldsymbol{x}}_c$ varies within $\mathbb{R}^2$, the right hand side of (2) spans a two-dimensional affine plane in $\mathbb{R}^6$, which is denoted P. For convenience, the forces in (1) are scaled such that $\|\boldsymbol{f}_g\| = 1$. Thus, the affine plane P is defined as

$$P = \left\{ \begin{pmatrix} \boldsymbol{e} \\ \tau \end{pmatrix} : \;\; \boldsymbol{e} \cdot \boldsymbol{\tau} = 0 \right\}. \tag{4}$$

Physically, P gives all the wrenches that balance the gravitational wrench for some center-of-mass horizontal position $\tilde{\boldsymbol{x}}_c$. Using the torque relation $\boldsymbol{\tau} = \boldsymbol{x}_c \times \boldsymbol{f}_g = \boldsymbol{e} \times \boldsymbol{x}_c$, any wrench $(\boldsymbol{f}, \boldsymbol{\tau}) \in P$ corresponds to a unique value of $\tilde{\boldsymbol{x}}_c$ according to

$$\tilde{\boldsymbol{x}}_c = -\mathbf{E}(\boldsymbol{e} \times \boldsymbol{\tau}). \tag{5}$$

The following key proposition utilizes the definitions of the wrench cone W and affine plane P in the wrench space in order to define the construction of the feasible region $\widetilde{\mathcal{R}}$.

Proposition 3.1. *Let a 3D object $\mathcal{B}$ be supported by n frictional contacts against gravity in three-dimensions. The equilibrium region $\widetilde{\mathcal{R}}$ is obtained as*

$$\widetilde{\mathcal{R}} = \{-\mathbf{E}(\boldsymbol{e} \times \boldsymbol{\tau}), \text{ for all } \begin{pmatrix} \boldsymbol{e} \\ \boldsymbol{\tau} \end{pmatrix} \in W \cap P\}, \tag{6}$$

where W is defined in (3) and P is defined in (4). Moreover, the boundary of $\widetilde{\mathcal{R}}$ is given by

$$\mathsf{bdy}(\widetilde{\mathcal{R}}) = \{-\mathbf{E}(\boldsymbol{e} \times \boldsymbol{\tau}), \text{ for all } \begin{pmatrix} \boldsymbol{e} \\ \boldsymbol{\tau} \end{pmatrix} \in \mathsf{bdy}(W) \cap P\}. \tag{7}$$

The rest of this section will thus follow the construction of $\widetilde{\mathcal{R}}$ as outlined in Proposition 3.1. First, the boundary of the wrench cone $\mathsf{bdy}(W)$ is analyzed and characterized. Next, the boundary of $\widetilde{\mathcal{R}}$ is constructed by computing the intersection $\mathsf{bdy}(W) \cap P$ and applying the linear map in (5). The construction is demonstrated graphically in computational examples in the next section.

The equilibrium region for frictionless contacts: We now briefly discuss the simple case where all contacts are frictionless, for which the equilibrium region $\widetilde{\mathcal{R}}$ is easily computed. In this case, the wrench cone W in (3) is a polyhedral convex cone of dimension $\mathsf{min}\{6, n\}$. Generically, the dimension of $\widetilde{\mathcal{R}}$ (if nonempty), which equals the dimension of $W \cap P$ is given by

$$\mathsf{dim}(\widetilde{\mathcal{R}}) = \mathsf{min}\{2, n-4\}. \tag{8}$$

That is, for $n \leq 3$ frictionless contacts $\widetilde{\mathcal{R}}$ is empty, for $n = 4$ contacts $\widetilde{\mathcal{R}}$ is a single point, for $n = 5$ contacts $\widetilde{\mathcal{R}}$ is a line segment, and for $n \geq 6$ contacts $\widetilde{\mathcal{R}}$ is a convex polygon. Special cases occur when one or more contacts are flat, i.e. $\boldsymbol{n}_i = \boldsymbol{e}$. In these non-generic cases, the formula (8) fails since the intersection of W and P is not transversal. An obvious example appears in Fig. 1(a) where $n = 4$ and all contacts are flat, so that $\widetilde{\mathcal{R}}$ is fully two-dimensional, in contrast to the prediction of a single point according to (8).

3.1 Computing the boundary of the wrench cone W

We now construct the boundary of the wrench cone W defined in (3), which is the cone of all possible wrenches that can be generated by the contact reaction forces. This is the most complicated part, which is at the core of this paper's contribution. Equation (3) implies that W is the image of a linear map $\mathcal{L}$, which is given by

$$\mathcal{L}: \mathcal{C} \to I\!R^6, \text{ where } \mathcal{C} = C_1 \times C_2 \times \ldots C_n \text{ and } \mathcal{L}(\boldsymbol{f}_1, \boldsymbol{f}_2, \ldots \boldsymbol{f}_n) = \sum_{i=1}^{n} \begin{pmatrix} \boldsymbol{f}_i \\ \boldsymbol{x}_i \times \boldsymbol{f}_i \end{pmatrix} \tag{9}$$

The domain of $\mathcal{L}$, denoted by $\mathcal{C}$, which is simply the cartesian product of all friction cones, is a stratified set that can be decomposed into *cells* (i.e. manifolds without a boundary), as follows. Each friction cone C_i, defined in (2) is decomposed as the disjoint union $C_i = O_i \cup I_i \cup S_i$, where $O_i = \{0\}$ is the cone's vertex point, I_i is the interior of C_i, and S_i is the

boundary of C_i excluding the vertex point. Using this notation, the domain $\mathcal{C}$ is decomposed into 3^n different cells, as given by

$$\mathcal{C} = (O_1 \cup I_1 \cup S_1) \times \cdots \times (O_n \cup I_n \cup S_n). \tag{10}$$

Each cell is represented by a choice of one component from $\{O_i, I_i, S_i\}$ for $i = 1 \ldots n$. Since the convex wrench cone W, which is the image of $\mathcal{C}$ under $\mathcal{L}$, is generically six-dimensional, its boundary is a stratified set whose pieces are manifolds with dimension 5 or less. In what follows, we focus on computing only the five-dimensional boundary pieces of W (generically, any boundary piece of lower dimension can be obtained as an intersection of several 5-dimensional boundary pieces). The following lemma characterizes the five-dimensional boundary pieces of W in terms of critical points of the map $\mathcal{L}$ in (9), as follows.

Lemma 3.2. *Let $\mathcal{K}$ be a cell of $\mathcal{C}$ as defined in (10). A five-dimensional boundary piece of W associated with $\mathcal{K}$ is a subset of points from the image of $\mathcal{K}$ under $\mathcal{L}$ which satisfy*

$$\mathsf{rank}(\mathsf{D}\mathcal{L}_\mathcal{K}) = 5, \tag{11}$$

where $D\mathcal{L}_\mathcal{K}$ is the Jacobian of the restriction of the map $\mathcal{L}$ to the cell $\mathcal{K}$.

Note that the rank condition in this lemma is only a *necessary* condition for a boundary (just like the derivative rule $f'(x) = 0$ is only a necessary condition for an extremum point of a scalar function $f(x)$). An additional condition which distinguishes the actual boundary points is given at a later stage in Theorem 2.

In order to make a concrete use of the characterization in Lemma 3.2, one has to choose a parametrization for each cell $\mathcal{K} \subset \mathcal{C}$ of dimension d, formulate the restricted map $\mathcal{L}_\mathcal{K}$ in terms of the chosen d parameters, and then compute the Jacobian matrix $D\mathcal{L}_\mathcal{K} \in \mathbb{R}^{6\times d}$ and find conditions for its rank deficiency. A cell $\mathcal{K}$ of dimension d can be assigned a suitable set of d parameters according to its components, S_i or I_i, as follows. A contact force $\boldsymbol{f}_i$ in an interior component I_i is parametrized simply by its cartesian coordinates in $\mathbb{R}^3$. A contact force $\boldsymbol{f}_i \in S_i$ is parametrized by the two scalars $(\lambda_i, \phi_i) \in \mathbb{R}^+ \times \mathbb{S}^1$, where $\lambda_i > 0$ is the force magnitude and ϕ_i is the force angle, measured by projecting $\boldsymbol{f}_i$ on the terrain's tangent plane at the contact $\boldsymbol{x}_i$. This plane is spanned by the unit vectors $\boldsymbol{s}_i$ and $\boldsymbol{t}_i$, such that $\{\boldsymbol{s}_i, \boldsymbol{t}_i, \boldsymbol{n}_i\}$ is a right-handed orthonormal frame. Using these parameters, a force $\boldsymbol{f}_i \in S_i$ is given by

$$\boldsymbol{f}_i(\lambda_i, \phi_i) = \lambda_i \boldsymbol{u}_i(\phi_i) \quad \text{such that} \quad \boldsymbol{u}_i(\phi_i) = \mu\cos(\phi_i)\boldsymbol{s}_i + \mu\sin(\phi_i)\boldsymbol{t}_i + \boldsymbol{n}_i \tag{12}$$

Since $\boldsymbol{u}_i(\phi_i)$ has a fixed magnitude, $\boldsymbol{u}_i'(\phi_i) = -\mu\sin(\phi_i)\boldsymbol{s}_i + \mu\cos(\phi_i)\boldsymbol{t}_i$ is orthogonal to $\boldsymbol{u}_i(\phi_i)$. The pair $\{\boldsymbol{u}_i(\phi_i), \boldsymbol{u}_i'(\phi_i)\}$ spans the *tangent plane* to S_i at $\boldsymbol{f}_i(\lambda_i, \phi_i)$, which will be denoted by $\Delta_i(\phi_i)$. Finally, we define $\boldsymbol{\eta}_i(\phi_i) = \boldsymbol{u}_i(\phi_i) \times \boldsymbol{u}_i'(\phi_i) = -\mu\cos(\phi_i)\boldsymbol{s}_i - \mu\sin(\phi_i)\boldsymbol{t}_i - \mu^2\boldsymbol{n}_i$, which is the outward-pointing normal to $\Delta_i(\phi_i)$ at $\boldsymbol{f}_i(\lambda_i, \phi_i)$. With a slight abuse of notation, we will also interpret $\Delta_i(\phi_i)$ as planes embedded in the *physical space*, that is, planes which are tangent to the friction cones C_i emanating from the contact points $\boldsymbol{x}_i$ in the three-dimensional space.

Next, the cells of $\mathcal{C}$ can be further divided into *classes*, in which the ordering of the contacts is ignored. For a given force cell $\mathcal{K}$ from (10), let n_S denote the number of choices of boundary components S_i, n_I denote the number of choices of interior components I_i, while the remaining $n - n_S - n_I$ components are O_i which represent contacts with zero force. There

are $\frac{1}{2}(n+1)(n+2)$ possible choices of n_S and n_I, each representing a different cell class. Each class can also be represented by a word from the alphabet $\{S, I\}$, where the first n_I letters are I and the following n_S letters are S. For example, for $n = 3$ contacts, cell class IS represents the six force cells: $O_1 \times S_2 \times I_3$, $O_1 \times I_2 \times S_3$, $S_1 \times O_2 \times I_3$, $I_1 \times O_2 \times S_3$, $S_1 \times I_2 \times O_3$ and $I_1 \times S_2 \times O_3$. Note that cells of a given class all have the same dimensionality which is the sum of the dimensions of their components, given by $2n_S + 3n_I$. For example, for $n = 3$ contacts, the cell classes with dimension of 5 or higher are IS, II, III, SII, ISS and SSS.

The following Lemma lists all cell classes of contact forces from $\mathcal{C}$ that possibly contribute to five-dimensional boundary pieces of the wrench cone W.

Lemma 3.3. *Given an arrangement of $n \geq 3$ contact points and their friction cones, the classes of cells of $\mathcal{C}$ whose image under the map $\mathcal{L}$ contains five-dimensional pieces of the boundary of the wrench cone W are: II, SI, SSI, SSS, $SSSS$ and $SSSSS$ only.*

A proof of this lemma, which relies on 3.2, appears in the Appendix.

The following theorem gives algebraic and geometric characterization of the sets of critical contact forces from all six cell classes listed in Lemma 3.3 that satisfy the condition $\mathsf{rank}(\mathsf{D}\mathcal{L}_\mathcal{K}) = 5$. The image of these critical forces under $\mathcal{L}$ contains all five-dimensional boundary pieces of the wrench cone W. For notational simplicity, we use the convention that forces at the first contacts with indices $1 \ldots n_S$ lie within the boundary components S_i while forces at the next contacts with indices $n_S + 1 \ldots n_S + n_I$ lie within the interior components I_i, and the rest of the contact forces with indices $n_S + n_I + 1 \ldots n$ are zero. This arbitrary choice of contact ordering represents all other possible permutations of contacts for any given cell class.

Theorem 1. *Consider a given arrangement of $n \geq 3$ contact points and their friction cones. For each of the contact force classes listed in Lemma 3.3, the necessary conditions for critical points that are mapped by $\mathcal{L}$ to candidate boundary points of W are:*
1. *Cell classes II and SI - the entire cells are critical points of $\mathcal{L}$, and their image under $\mathcal{L}$ is a subset of a five-dimensional linear subspace of $\mathbb{R}^6$. Geometrically, it represents wrenches that generate zero moment about the line connecting the contacts $\boldsymbol{x}_1$ and $\boldsymbol{x}_2$.*
2. *Cell class SSI — The cell is 7-dimensional, and is parametrized by $\boldsymbol{f}_3 \in \mathbb{R}^3$ and the pairs (λ_1, ϕ_1) and (λ_2, ϕ_2), giving rise to 7 scalar parameters. The critical points of $\mathcal{L}$ within the cell are described by the two scalar relations*

$$\begin{aligned} \boldsymbol{\eta}_1(\phi_1) \cdot (x_2 - x_3) &= 0 \\ \boldsymbol{\eta}_2(\phi_2) \cdot (x_2 - x_3) &= 0. \end{aligned} \tag{13}$$

Conditions (13) imply that the angles ϕ_1 and ϕ_2 are constant while the magnitudes λ_1 and λ_2 and the contact force $\boldsymbol{f}_3 \in I_3$ vary freely within the cell. Thus, (13) defines a five-dimensional set of critical points. Furthermore, for any particular solution ϕ_1^*, ϕ_2^* of (13), this set is a five-dimensional linear subspace of $\mathbb{R}^6$. The geometric interpretation of (13) is that the angles ϕ_1^* and ϕ_2^* are chosen such that the tangent planes $\Delta_1(\phi_1^*)$ and $\Delta_2(\phi_2^*)$ of the physical friction cones C_1 and C_2 both contain the contact point $\boldsymbol{x}_3$. There are up to 2 solutions for each angle ϕ_1, ϕ_2 in (13), giving rise to four different linear subspaces of $\mathbb{R}^6$. Each of these linear subspaces contains wrenches that generate zero moment about the line of intersection of the planes $\Delta_1(\phi_1^*)$ and $\Delta_2(\phi_2^*)$.

3. *Cell class SSS — The cell is 6-dimensional, and is parametrized by the three pairs* (λ_i, ϕ_i) *for* $i = 1, 2, 3$. *The critical points of* $\mathcal{L}$ *within the cell are described by the scalar relation*

$$\det \begin{bmatrix} \bar{\boldsymbol{s}}\cdot\boldsymbol{\nu}_1(\phi_1) & \bar{\boldsymbol{s}}\cdot\boldsymbol{\nu}_2(\phi_2) & \bar{\boldsymbol{s}}\cdot\boldsymbol{\nu}_3(\phi_3) \\ \bar{\boldsymbol{t}}\cdot\boldsymbol{\nu}_1(\phi_1) & \bar{\boldsymbol{t}}\cdot\boldsymbol{\nu}_2(\phi_2) & \bar{\boldsymbol{t}}\cdot\boldsymbol{\nu}_3(\phi_3) \\ \bar{\boldsymbol{n}}\cdot(x_1\times\boldsymbol{\nu}_1(\phi_1)) & \bar{\boldsymbol{n}}\cdot(x_2\times\boldsymbol{\nu}_2(\phi_2)) & \bar{\boldsymbol{n}}\cdot(x_3\times\boldsymbol{\nu}_3(\phi_3)) \end{bmatrix} = 0 \tag{14}$$

where $\boldsymbol{\nu}_i(\phi_i) = \bar{\boldsymbol{n}}\times\boldsymbol{\eta}_i(\phi_i)$, $\bar{\boldsymbol{n}}$ *is a unit vector normal to the plane* Δ_{123} *which passes through the three contact points* $\{\boldsymbol{x}_1, \boldsymbol{x}_2, \boldsymbol{x}_3\}$, *and the unit vectors* $\bar{\boldsymbol{s}}$ *and* $\bar{\boldsymbol{t}}$ *are tangent to that plane, such that* $\{\bar{\boldsymbol{s}}, \bar{\boldsymbol{t}}, \bar{\boldsymbol{n}}\}$ *is an orthonormal frame. The condition (14) implies that the three angles* $\{\phi_1, \phi_2, \phi_3\}$ *lie on a two-dimensional manifold while the three magnitudes* $\{\lambda_1, \lambda_2, \lambda_3\}$ *vary freely, thus the critical points are forming a five-dimensional manifold. The geometric interpretation of (14) is that the angles* $\{\phi_1, \phi_2, \phi_3\}$ *are chosen such that the intersection point of the three tangent planes* $\Delta_1(\phi_1)$, $\Delta_2(\phi_2), \Delta_3(\phi_3)$ *to the physical friction cones* C_1, C_2, C_3 *lies within the plane* Δ_{123}.

4. *Cell class SSSS — The cell is 8-dimensional, and is parametrized by the four pairs* (λ_i, ϕ_i) *for* $i = 1, 2, 3, 4$. *The critical points of* $\mathcal{L}$ *within the cell are described by angles* ϕ_i *that satisfy three scalar equations of the form*

$$\det \begin{bmatrix} \bar{\boldsymbol{s}}\cdot\boldsymbol{\nu}_a(\phi_a) & \bar{\boldsymbol{s}}\cdot\boldsymbol{\nu}_b(\phi_b) & \bar{\boldsymbol{s}}\cdot\boldsymbol{\nu}_c(\phi_c) \\ \bar{\boldsymbol{t}}\cdot\boldsymbol{\nu}_a(\phi_a) & \bar{\boldsymbol{t}}\cdot\boldsymbol{\nu}_b(\phi_b) & \bar{\boldsymbol{t}}\cdot\boldsymbol{\nu}_c(\phi_c) \\ \bar{\boldsymbol{n}}\cdot(x_a\times\boldsymbol{\nu}_a(\phi_a)) & \bar{\boldsymbol{n}}\cdot(x_b\times\boldsymbol{\nu}_b(\phi_b)) & \bar{\boldsymbol{n}}\cdot(x_c\times\boldsymbol{\nu}_c(\phi_c)) \end{bmatrix} = 0 \tag{15}$$

where the indices $a < b < c$ *are chosen from the set* $\{1, 2, 3, 4\}$, $\boldsymbol{\nu}_i(\phi_i) = \bar{\boldsymbol{n}}\times\boldsymbol{\eta}_i(\phi_i)$, $\bar{\boldsymbol{n}}$ *is a unit vector normal to the plane* Δ_{abc} *which passes through the three contact points* $\{\boldsymbol{x}_a, \boldsymbol{x}_b, \boldsymbol{x}_c\}$, *and the unit vectors* $\bar{\boldsymbol{s}}$ *and* $\bar{\boldsymbol{t}}$ *are tangent to that plane, such that* $\{\bar{\boldsymbol{s}}, \bar{\boldsymbol{t}}, \bar{\boldsymbol{n}}\}$ *is an orthonormal frame. Using these three equations, the four angles* ϕ_i *lie in a one-dimensional manifold while the four magnitudes* λ_i *vary freely, giving rise to a five-dimensional set of critical points. Equivalently, The angles* ϕ_i *can be characterized by the existence of* $\boldsymbol{\omega}, \boldsymbol{v} \in \mathbb{R}^3$ *such that* $||\boldsymbol{v}||^2 + ||\boldsymbol{\omega}||^2 > 0$, *which satisfy*

$$\boldsymbol{v}\cdot\boldsymbol{u}_i(\phi_i) + \boldsymbol{\omega}\cdot(\boldsymbol{x}_i\times\boldsymbol{u}_i(\phi_i)) = 0 \text{ and } \boldsymbol{v}\cdot\boldsymbol{u}_i'(\phi_i) + \boldsymbol{\omega}\cdot(\boldsymbol{x}_i\times\boldsymbol{u}_i'(\phi_i)) = 0 \tag{16}$$

for $i = 1, 2, 3, 4$.

5. *Cell class SSSSS — The cell is 10-dimensional, and is parametrized by the five pairs* (λ_i, ϕ_i) *for* $i = \{1..5\}$. *The critical points of* $\mathcal{L}$ *within the cell are described by angles* ϕ_i *that satisfy five scalar equations of the form (15) where the indices* $a < b < c$ *are chosen from the set* $\{1, 2, 3, 4, 5\}$. *Using these five equations gives a finite number of solutions for the five angles* ϕ_i, *which are held fixed while the the five magnitudes* λ_i *vary freely. Thus, the set of critical points within the cell is a five-dimensional set. Furthermore, for each particular solution for the angles* ϕ_i, *this set is a five-dimensional linear subspace of* $\mathbb{R}^6$. *Equivalently, The angles* ϕ_i *can be characterized by the existence of* $\boldsymbol{\omega}, \boldsymbol{v} \in \mathbb{R}^3$ *such that* $||\boldsymbol{v}||^2 + ||\boldsymbol{\omega}||^2 > 0$, *which satisfy (16) for* $i = 1, 2, 3, 4, 5$.

A proof of Theorem 1 appears in the Appendix. Importantly, the conditions which define critical points of $\mathcal{L}$ given in Theorem 1 are only *necessary* for finding points on the boundary of the wrench cone W. That is, a critical point in a force cell $\mathcal{K} \subset \mathcal{C}$ can possibly be mapped under $\mathcal{L}_\mathcal{K}$ to a point in the *interior* of W. The following Lemma complements the criticality

conditions with a *sufficient condition* which characterizes critical points that map to the actual boundary of W.

Lemma 3.4. *Let $\mathcal{K}$ be a cell of $\mathcal{C}$ as defined in (10), and let $\boldsymbol{f}^* \in \mathcal{K}$ be a critical point of $\mathcal{L}_\mathcal{K}$ which satisfies the criticality condition (11). The image point $\boldsymbol{w}^* = \mathcal{L}(\boldsymbol{f}^*)$ lies on the boundary of W if there exists a five-dimensional separating hyperplane $H \subset \mathbb{R}^6$ passing through $\boldsymbol{w}^*$, such that all points $\boldsymbol{w} \in W$ lie* on the same side *of H. That is, there exists a sign $\sigma \in \{-1, +1\}$ that satisfies*

$$\sigma(\boldsymbol{w} \cdot \boldsymbol{\eta}_H) \geq 0 \;\; \textit{for all } \boldsymbol{w} \in W, \tag{17}$$

where $\boldsymbol{\eta}_H$ is the normal to the hyperplane H in $\mathbb{R}^6$.

A key observation is that for each cell class $\mathcal{K}$ listed in Lemma 3.3, the criticality conditions in Theorem 1 already imply the existence of a five-dimensional hyperplane H which is *locally tangent* to the image of $\mathcal{L}_\mathcal{K}$ at a given candidate boundary point $\boldsymbol{w}^* \in W$. Thus, one only needs to check whether the hyperplane H satisfies the separation condition given in (17). The following theorem utilizes this observation in order to give concrete conditions that describe the actual boundary of W.

Theorem 2. *Consider a given arrangement of $n \geq 3$ contact points and their friction cones. For each cell class $\mathcal{K} \subset \mathcal{C}$ listed in Lemma 3.3, conditions for critical points within $\mathcal{K}$ whose image under the map $\mathcal{L}_\mathcal{K}$ lies on the actual boundary of the wrench cone W are given as follows:*

1. *Cell classes SS and SI — the entire image of the cell under $\mathcal{L}_\mathcal{K}$ lies on the boundary of W if and only if there exists a sign $\sigma \in \{-1, +1\}$ that satisfies*

$$\sigma\left((\boldsymbol{x}_2 - \boldsymbol{x}_1) \cdot (\boldsymbol{x}_i - \boldsymbol{x}_1) \times \boldsymbol{u}_i(\phi_1)\right) \geq 0 \textit{ for all } \phi_i \in \mathbb{S}^1 \textit{ and } i \in \{3 \dots n\}. \tag{18}$$

In particular, for a **tame** *contact arrangement, if the projected contacts $\tilde{\boldsymbol{x}}_1, \tilde{\boldsymbol{x}}_2$ are two adjacent vertices of the support polygon Π, then condition (18) is necessarily satisfied.*

2. *Cell class SSI — a critical point within the cell class is associated with fixed values of the angles $\phi_1 = \phi_1^*$ and $\phi_2 = \phi_2^*$, that are determined by the conditions in (13). The image of the critical point under $\mathcal{L}$ lies on the boundary of W if and only if there exists a sign $\sigma \in \{-1, +1\}$ which satisfies*

$$\begin{aligned} &\sigma(\boldsymbol{\nu}_{12} \cdot (\boldsymbol{x}_1 - \boldsymbol{x}_3) \times \boldsymbol{n}_1) \geq 0, \;\; \sigma(\boldsymbol{\nu}_{12} \cdot (\boldsymbol{x}_2 - \boldsymbol{x}_3) \times \boldsymbol{n}_2) \geq 0 \\ &\textit{and } \sigma\left(\boldsymbol{\nu}_{12} \cdot (\boldsymbol{x}_i - \boldsymbol{x}_3) \times \boldsymbol{u}_i(\phi_i)\right) \geq 0 \textit{ for all } \phi_i \in \mathbb{S}^1 \textit{ and } i \in \{4 \dots n\}, \\ &\textit{where } \nu_{12} = \boldsymbol{\eta}_1(\phi_1^*) \times \boldsymbol{\eta}_2(\phi_2^*). \end{aligned} \tag{19}$$

3. *Cell class SSS — a critical point of $\mathcal{L}$ within the cell is associated with angles ϕ_1, ϕ_2 and ϕ_3 that satisfy the relation (14). Let $\boldsymbol{z}$ denote the intersection point of the three planes $\Delta_i(\phi_i)$ which are tangent to the friction cones C_i in physical space. According to Theorem 1, the point $\boldsymbol{z}$ must lie on the plane Δ_{123} passing through the contacts points $\boldsymbol{x}_1, \boldsymbol{x}_2$ and $\boldsymbol{x}_3$, whose normal is denoted by $\bar{\boldsymbol{n}}$. The image of a critical point under $\mathcal{L}$ lies on the boundary of W if and only if there exists a sign $\sigma \in \{-1, +1\}$ which satisfies*

$$\begin{aligned} &\sigma\big(\bar{\boldsymbol{n}} \cdot ((\boldsymbol{x}_1 - \boldsymbol{z}) \times \boldsymbol{n}_1)\big) \geq 0, \; \sigma\big(\bar{\boldsymbol{n}} \cdot ((\boldsymbol{x}_2 - \boldsymbol{z}) \times \boldsymbol{n}_2)\big) \geq 0, \; \sigma\big(\bar{\boldsymbol{n}} \cdot ((\boldsymbol{x}_3 - \boldsymbol{z}) \times \boldsymbol{n}_3)\big) \geq 0 \\ &\textit{and } \; \sigma\big(\bar{\boldsymbol{n}} \cdot ((\boldsymbol{x}_i - \boldsymbol{z}) \times \boldsymbol{u}_i(\phi_i))\big) \geq 0 \textit{ for all } \phi_i \in \mathbb{S}^1 \textit{ and } i \in \{4 \dots n\}. \end{aligned} \tag{20}$$

4. *Cell class SSSS — a critical point of $\mathcal{L}$ within the cell is associated with angles ϕ_i for which there exist $\boldsymbol{\omega}, \boldsymbol{v} \in I\!R^3$ that satisfy the relation (16) for $i = 1, 2, 3, 4$. The image of a critical point under $\mathcal{L}$ lies on the actual boundary of W if and only if there exists a sign $\sigma \in \{-1, +1\}$ which satisfies*

$$\begin{aligned} &\sigma\big(\boldsymbol{v} \cdot \boldsymbol{n}_i + \boldsymbol{\omega} \cdot (\boldsymbol{x}_i \times \boldsymbol{n}_i)\big) \geq 0 \text{ for } i = 1, 2, 3, 4, \text{ and} \\ &\sigma\big(\boldsymbol{v} \cdot \boldsymbol{u}_i(\phi_i) + \boldsymbol{\omega} \cdot (\boldsymbol{x}_i \times \boldsymbol{u}_i(\phi_i))\big) \geq 0 \text{ for all } \phi_i \in \mathbb{S}^1 \text{ and } i \in \{5 \dots n\}. \end{aligned} \tag{21}$$

5. *Cell class SSSSS — a critical point of $\mathcal{L}$ within the cell is associated with angles ϕ_i for which there exist $\boldsymbol{\omega}, \boldsymbol{v} \in I\!R^3$ which satisfy the relation (16) for $i = 1 \dots 5$. The image of the critical point under $\mathcal{L}$ lies on the actual boundary of W if and only if there exists a sign $\sigma \in \{-1, +1\}$ which satisfies*

$$\begin{aligned} &\sigma\big(\boldsymbol{v} \cdot \boldsymbol{n}_i + \boldsymbol{\omega} \cdot (\boldsymbol{x}_i \times \boldsymbol{n}_i)\big) \geq 0 \text{ for } i = 1 \dots 5, \text{ and} \\ &\sigma\big(\boldsymbol{v} \cdot \boldsymbol{u}_i(\phi_i) + \boldsymbol{\omega} \cdot (\boldsymbol{x}_i \times \boldsymbol{u}_i(\phi_i))\big) \geq 0 \text{ for all } \phi_i \in \mathbb{S}^1 \text{ and } i \in \{6 \dots n\}. \end{aligned} \tag{22}$$

A proof of Theorem 2 appears in the Appendix. Note that all the conditions mentioned above require checking the sign of an expression of the form $\boldsymbol{v} \cdot \boldsymbol{u}_i(\phi_i) + \boldsymbol{\omega} \cdot (\boldsymbol{x}_i \times \boldsymbol{u}_i(\phi_i))$ for all $\phi_i \in \mathbb{S}^1$. This check can be reduced to computing extremum values of a function of the form $g(\phi_i) = a_i + b_i \cos\phi_i + c_i \sin\phi_i$, which can be found explicitly.

3.2 Computing the boundary of $\widetilde{\mathcal{R}}$

We now combine the results of Theorems 1 and 2 that characterize the boundary of the wrench cone W with the construction given in (7) in order to compute the boundary of the equilibrium region $\widetilde{\mathcal{R}}$. The boundary of $\widetilde{\mathcal{R}}$ is a closed curve in $I\!R^2$ which consists of a concatenation of pieces of five possible types, each are associated with boundary pieces of the wrench cone W. The following theorem summarizes the formulation of the five types of boundary curves of $\widetilde{\mathcal{R}}$. For simplicity, each boundary curve is formulated under an arbitrary assignment of indices to the contacts and contact forces, but represents the family of curves obtained by applying all possible index permutations.

Theorem 3. *Given an arrangement of $n \geq 3$ contact points and their friction cones, the horizontal cross-section of its equilibrium region $\widetilde{\mathcal{R}}$ is bounded by up to* **five** *possible types of curves:*

1. **Two-contact SI/SS segment:** *a linear segment lying on the line $\tilde{x}_1 - \tilde{x}_2$, which is associated with nonzero contact forces $\boldsymbol{f}_1$ and $\boldsymbol{f}_2$ while $\boldsymbol{f}_i = \vec{0}$ for $i \in \{3 \dots n\}$. The endpoints of this linear segment can be obtained by solving a linear program for $\tilde{\boldsymbol{x}}_c, \boldsymbol{f}_1, \boldsymbol{f}_2$ under the equilibrium equation (1) and the linear inequality constraints $\boldsymbol{f}_i \in C_i \cap V_{12}$ for $i = 1, 2$, where V_{12} is the plane spanned by the vertical direction $\boldsymbol{e}$ and the line $\tilde{x}_2 - \tilde{x}_1$.*

2. **Three-contact SSI segments:** *linear segment associated with contact forces $\boldsymbol{f}_1 \in S_1$, $\boldsymbol{f}_2 \in S_2$ and $\boldsymbol{f}_3 \in I_3$ while $\boldsymbol{f}_i = 0$ for all $i \in \{4 \dots n\}$. The forces $\boldsymbol{f}_1$ and $\boldsymbol{f}_2$ are parametrized as $\boldsymbol{f}_i = \lambda_1 \boldsymbol{u}_i(\phi_i^*)$ for $i = 1, 2$, where ϕ_1^*, ϕ_2^* are solutions of equation (13)*

that also satisfy the separation condition (19). Geometrically, an SSI segment lies on the horizontal projection of the line of intersection of the two planes $\Delta_1(\phi_1^*)$ and $\Delta_2(\phi_2^*)$ tangent to the friction cones C_i emanating at the contacts $\boldsymbol{x}_1$ and $\boldsymbol{x}_2$. The endpoints of an SSI segment can be obtained by solving a linear program for $\tilde{\boldsymbol{x}}_c, \lambda_1, \lambda_2, \boldsymbol{f}_3$ under the equilibrium equation (1) and the inequality constraints $\lambda_1, \lambda_2 \geq 0$ and $\boldsymbol{f}_3 \in C_3 \cap P_3$, where P_3 is the plane spanned by the vertical direction $\boldsymbol{e}$ and the horizontal direction $\mathbf{E}^T(\tilde{\boldsymbol{r}}_{12} - \tilde{\boldsymbol{x}}_3)$, where $\boldsymbol{r}_{12}$ is the intersection point of a horizontal line emanating from $\boldsymbol{x}_1$ in the direction $\mathbf{E}\boldsymbol{u}_1(\phi_1^*)$ and a horizontal line emanating from $\boldsymbol{x}_2$ in the direction $\mathbf{E}\boldsymbol{u}_2(\phi_2^*)$.

3. **Three-contact SSS curve:** *a nonlinear curve associated with contact forces $\boldsymbol{f}_i \in S_i$ for $i = 1, 2, 3$. The forces are parametrized by λ_i, ϕ_i, where the angles (ϕ_1, ϕ_2, ϕ_3) lie on the one-dimensional solution set of equation (14) combined with the equation:*

$$\det \begin{bmatrix} \mathbf{E}\boldsymbol{u}_1(\phi_1) & \mathbf{E}\boldsymbol{u}_2(\phi_2) & \mathbf{E}\boldsymbol{u}_3(\phi_3) \\ \boldsymbol{e}\cdot(\boldsymbol{x}_1 \times \boldsymbol{u}_1(\phi_1)) & \boldsymbol{e}\cdot(\boldsymbol{x}_2 \times \boldsymbol{u}_2(\phi_2)) & \boldsymbol{e}\cdot(\boldsymbol{x}_3 \times \boldsymbol{u}_3(\phi_3)) \end{bmatrix} = 0 \tag{23}$$

Geometrically, (23) implies that the lines of the three contact forces intersect a common vertical line, while (14) implies that the intersection point of the three tangent planes $\Delta_1(\phi_1), \Delta_2(\phi_2), \Delta_3(\phi_3)$ lies on the plane spanned by $\boldsymbol{x}_1$, $\boldsymbol{x}_2$, and $\boldsymbol{x}_3$. Each particular solution of (23) and (14) for ϕ_1, ϕ_2, ϕ_3 which also satisfies the separation condition (20) for some $\sigma \in \{-1, +1\}$, is associated with a potential point $\tilde{\boldsymbol{x}}_c$ on the boundary of $\widetilde{\mathcal{R}}$, as follows. First, the magnitudes λ_i are obtained by solving the 3×3 linear system:

$$\lambda_1 \boldsymbol{u}_1(\phi_1) + \lambda_2 \boldsymbol{u}_2(\phi_2) + \lambda_3 \boldsymbol{u}_3(\phi_3) = \boldsymbol{e} \tag{24}$$

Only if the solution of (24) satisfies $\lambda_i \geq 0$ for $i = 1, 2, 3$, then it contributes a point $\tilde{\boldsymbol{x}}_c$ on the boundary of $\widetilde{\mathcal{R}}$, which is obtained as:

$$\tilde{\boldsymbol{x}}_c = -\mathbf{E}\left(\boldsymbol{e} \times (\lambda_1 \boldsymbol{x}_1 \times \boldsymbol{u}_1(\phi_1) + \lambda_2 \boldsymbol{x}_2 \times \boldsymbol{u}_2(\phi_2) + \lambda_3 \boldsymbol{x}_3 \times \boldsymbol{u}_3(\phi_3))\right). \tag{25}$$

4. **Four-contact SSSS curve:** *a nonlinear curve associated with contact forces $\boldsymbol{f}_i \in S_i$ for $i = 1, 2, 3, 4$. The forces are parametrized by λ_i, ϕ_i, where the angles $\phi_1 \ldots \phi_4$ lie on the one-dimensional solution set of three scalar equations of the form (15) where the indices $a < b < c$ are chosen from the set $\{1, 2, 3, 4\}$. Each particular solution for ϕ_i which also satisfies the separation condition (21) for some $\sigma \in \{-1, +1\}$, is associated with a potential point $\tilde{\boldsymbol{x}}_c$ on the boundary of $\widetilde{\mathcal{R}}$, as follows. First, the magnitudes λ_i are obtained by solving the 4×4 linear system:*

$$\begin{cases} \lambda_1 \boldsymbol{u}_1(\phi_1) + \lambda_2 \boldsymbol{u}_2(\phi_2) + \lambda_3 \boldsymbol{u}_3(\phi_3) + \lambda_1 \boldsymbol{u}_1(\phi_1) = \boldsymbol{e} \\ \boldsymbol{e} \cdot (\lambda_1 \boldsymbol{x}_1 \times \boldsymbol{u}_1(\phi_1) + \lambda_2 \boldsymbol{x}_2 \times \boldsymbol{u}_2(\phi_2) + \lambda_3 \boldsymbol{x}_3 \times \boldsymbol{u}_3(\phi_3) + +\lambda_4 \boldsymbol{x}_4 \times \boldsymbol{u}_4(\phi_4)) = 0. \end{cases} \tag{26}$$

Only if the solution of (26) satisfies $\lambda_i \geq 0$ for $i = 1, 2, 3, 4$, then it contributes a point $\tilde{\boldsymbol{x}}_c$ on the boundary of $\widetilde{\mathcal{R}}$, which is obtained as:

$$\tilde{\boldsymbol{x}}_c = -\mathbf{E}\left(\boldsymbol{e} \times \left(\sum_{i=1}^{4} \lambda_i \boldsymbol{x}_i \times \boldsymbol{u}_i(\phi_i)\right)\right). \tag{27}$$

5. **Five-contact SSSSS segments:** *linear segments associated with contact forces* $\boldsymbol{f}_i \in S_i$ *for* $i = 1, 2, 3, 4, 5$. *The forces are parametrized by* λ_i, ϕ_i, *where the angles* ϕ_i *are solutions of a system of five scalar equations of the form (15) where the indices* $a < b < c$ *are chosen from the set* $\{1, 2, 3, 4, 5\}$. *This system admits a finite number of solutions for the angles* $\phi_1 \ldots \phi_5$. *Each solution which satisfies the separation condition (22) for some* $\sigma \in \{-1, +1\}$, *is associated with a line segment of* $\tilde{\boldsymbol{x}}_c$ *values on the boundary of* $\widetilde{\mathcal{R}}$. *This line segment is obtained by solving a linear program for* $\tilde{\boldsymbol{x}}_c, \lambda_i$ *under the equilibrium equation (1) and the linear inequalities* $\lambda_i \geq 0$.

A proof of the theorem appears in the Appendix.

Remarks on practical computation of the boundary of $\widetilde{\mathcal{R}}$: We now briefly discuss practical computational aspects of implementing the recipe given in Theorem 3 for computing the boundary of the equilibrium region $\widetilde{\mathcal{R}}$. As seen from the theorem, boundary curves of types 1 and 2 are linear segments with a clear geometric meaning, and their endpoints can be easily obtained by solving a low-dimensional linear programming problem.

Boundary curve of type 3 (SSS) is a nonlinear curve whose computation is based on finding the one-dimensional solution set of the two equations (14) and (23) which are trigonometric in the angles ϕ_1, ϕ_2, ϕ_3. Using the substitution $\beta_i = \tan(\phi_i/2)$, these equations can be transformed to a system of two polynomial equations of degree 6 in β_i. In [Or, Phd Thesis 2007], it is further shown that dialytic elimination technique can be used to reduce these two equations into a single polynomial of degree 16 in two variables β_1, β_2, where each variable appears in degree 8. This equation can then be solved numerically by running β_1 (or ϕ_1) on a series of discrete values, finding the real roots of an eight-degree polynomial for β_2 numerically, and then solving a quadratic equation for the eliminated β_3. An alternative approach for computing a solution curve of (14) and (23) is to start from a known solution point (ϕ_1, ϕ_2, ϕ_3) and trace the solution curve numerically by marching along its tangent vector which is obtained by differentiation of (14) and (23) as implicit functions. Finding a starting point on the solution curve is sometimes possible due to the fact that endpoints of type 3 boundary curves often coincide with endpoints of type 1 and type 2 boundary segments, which are easily obtained. In case where no type 1 or type 2 segments exist on the boundary of $\widetilde{\mathcal{R}}$, one can find a starting point on the boundary by solving a single query of a convex programming problem of maximizing the projection of $\tilde{\boldsymbol{x}}_c$ along a specific direction in $\mathbb{R}^2$ (see [Bretl and Lall, 2008] for example).

Boundary curve of type 4 (SSSS) is a nonlinear curve whose computation is based on finding the one-dimensional solution set of three equations which are trigonometric in the angles $\phi_1, \phi_2, \phi_3, \phi_4$. Using the substitution $\beta_i = \tan(\phi_i/2)$, these equations can be transformed to a system of three polynomial equations of degree 6 in β_i. Using dialytic elimination, these three equations can be reduced into a single polynomial of degree 32 in two variables β_1, β_2, where each variable appears in degree 16 (unpublished work). This equation can then be solved numerically by running β_1 (or ϕ_1) on a series of discrete values, finding the real roots of the 16-degree polynomial for β_2 numerically, and then solving two quadratic equations for the eliminated variables β_3 and β_4. Again, the solution curve can alternatively be computed by numerical tracing along its tangent. As for finding a starting point $(\phi_1 \ldots \phi_4)$ lying on the curve, an important observation is as follows. When tracing the type-3 solution curve in (ϕ_1, ϕ_2, ϕ_3) space while checking the separation condition (20), a point where the second inequality in (20) crosses zero for some $i = k$ precisely coincides with

a point where $(\phi_1, \phi_2, \phi_3, \phi_k)$ lies on type-4 solution curve. That is, starting point of type 4 boundary curves often lie on endpoints of type 3 curves where the separation inequality condition vanishes.

Boundary segments of type 5 (SSSSS) require solving a system of five trigonometric equations in the five angles $\phi_1 \dots \phi_5$. Using the substitution $\beta_i = \tan(\phi_i/2)$ and transforming to polynomial equations, Bézout's theorem implies that maximal number of possible solutions to this system is 6^5. Finding all possible solutions is extremely complicated due to the high dimensionality. Nevertheless, an important observation is that any endpoint of a type 5 linear segment, where one contact force vanishes, must be an endpoint of a type 4 curve, precisely where the second inequality in the separation condition (21) crosses zero. Thus, there is no need to explicitly solve for $\phi_1 \dots \phi_5$, and type 5 segments can be simply obtained by connecting endpoints of type 4 curves by straight line segments.

Next, the following proposition which is stemming directly from Theorem 3 states that the equilibrium region for a tame arrangement of $n > 4$ contacts can be constructed from considering all possible 4-tuples of contacts.

Proposition 3.5. *Consider a tame arrangement of $n > 4$ contact points and their friction cones. The equilibrium region $\widetilde{\mathcal{R}}$ can be constructed as*

$$\widetilde{\mathcal{R}} = \mathsf{conv}\left\{\widetilde{\mathcal{R}}_{ijkl}, i < j < k < l \in \{1 \dots n\}\right\}, \tag{28}$$

where conv *denotes the convex hull and $\widetilde{\mathcal{R}}_{ijkl}$ is the equilibrium region associated with only the four contacts $\boldsymbol{x}_i, \boldsymbol{x}_j, \boldsymbol{x}_k, \boldsymbol{x}_l$.*

This proposition is analogous to the statement in [Or and Rimon, 2006] that in two dimensions, the equilibrium region can be constructed by taking convex hull of all regions associated with any *pair* of contacts.

3.3 Onset of non-static contact motions

According to Theorem 3, the boundary of the equilibrium region $\widetilde{\mathcal{R}}$ consists of five types of curves, each associated with critical contact forces from a different cell class. When the center-of-mass slowly moves such that its horizontal projection crosses the boundary of $\widetilde{\mathcal{R}}$, static equilibrium can no longer be maintained and a non-static motion begins to evolve. Importantly, the interactions at the contacts in this imminent motion are dictated by the type of the boundary curve of $\widetilde{\mathcal{R}}$ which has been crossed and its associated force cell $\mathcal{K}$, as follows. If the force cell $\mathcal{K}$ contains a component of zero contact force O_i then the body breaks contact at $\boldsymbol{x}_i$ and the force $\boldsymbol{f}_i$ vanishes. If the force cell $\mathcal{K}$ contains a component S_i of contact force $\boldsymbol{f}_i$ that lies on the friction cone boundary S_i then the contact at $\boldsymbol{x}_i$ is slipping. Finally, if the force cell $\mathcal{K}$ contains a component I_i of contact force $\boldsymbol{f}_i$ lying within the interior of the friction cone then body rolls about the contact at $\boldsymbol{x}_i$ which is kept stationary. Therefore, crossing each of the five types of boundary curves of $\widetilde{\mathcal{R}}$ can be associated to the onset of a particular mode of non-static motion, listed as follows. Crossing type 1 boundary segment associated with force cell class **SI** corresponds to tip-over motion of rolling about the line connecting two stationary contacts while all other contacts are separating. Crossing type 2 boundary segment associated with force cell class **SSI** corresponds to rolling about a single stationary contact while two other contacts are slipping while all other contacts (if

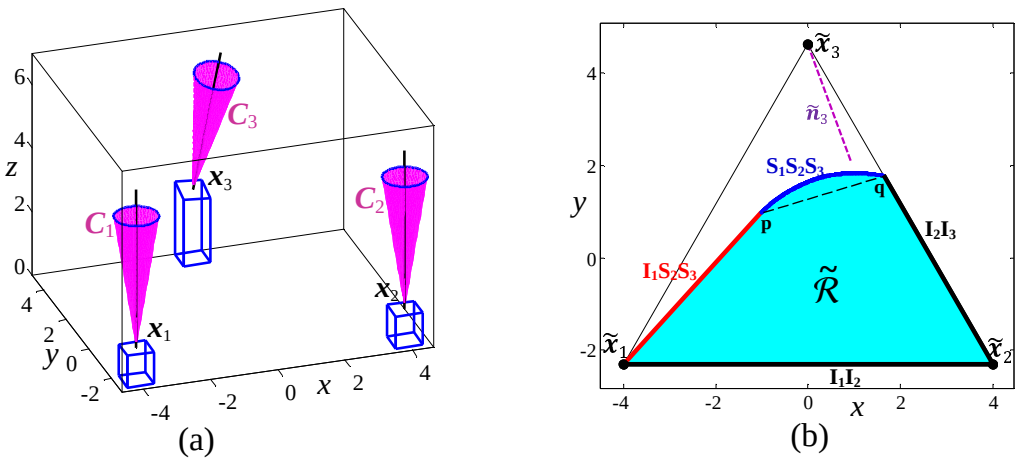

Figure 2: (a) The 3-contact arrangement in 3D. (b) Top view of the feasible equilibrium region $\widetilde{\mathcal{R}}$ and its three types of boundary curves.

they exist) are separating. Finally, crossing boundary curves of types 3,4, and 5 which are associated with force cell classes **SSS**, **SSSS** and **SSSSS** leads to onset of slippage at 3,4 or 5 contacts, while all other contacts (if they exist) are separating.

4 Computational examples

This section presents graphical examples of computing the equilibrium region $\widetilde{\mathcal{R}}$ for tame arrangements of 3,4, and 5 frictional contacts. The coordinates of all contact locations are given by cylindrical coordinates as $\boldsymbol{x}_i = (x_i, y_i, z_i) = (r\cos\phi_i, r\sin\phi_i, z_i)$ for $i = 1 \ldots n$. The contact normals are expressed by $x{-}z$ rotation angles as $\boldsymbol{n}_i = (\sin\alpha_i \sin\beta_i, -\cos\alpha_i \sin\beta_i, \cos\beta_i)$, and a uniform friction coefficient μ is assumed at all contacts. The following computational examples involve arrangements of three, four and five contacts with uniform friction coefficient. The data of these contact arrangements is identical to the setup of the three experiments which are presented in the next section.

Computational example - three contacts: the three contact locations are given by $r = 8/\sqrt{3}$, $\phi_i = \{-150°, -30°, 90°\}$ and $z_i = \{1, 1, 1 + r/4\}$. The contact normals' angles are given by $\alpha_i = \{0°, 0°, 20°\}$ and $\beta_i = \{0°, 0°, 15°\}$, and the friction coefficient at all contacts is 0.155. This contact arrangement, which is shown in Figure 2(a), can be verified as being tame. Nevertheless, since the contact $\boldsymbol{x}_3$ is not quasi-flat it must satisfy $\tilde{\boldsymbol{x}}_3 \notin \widetilde{\mathcal{R}}$, and according to Proposition 2.2 the equilibrium region is strictly contained in the support polygon $\widetilde{\mathcal{R}} \subset \Pi$. Figure 2(b) plots the equilibrium region $\widetilde{\mathcal{R}}$ for this contact arrangement in xy plane, whose boundary is computed according to Theorem 3. The boundary of $\widetilde{\mathcal{R}}$ consists of two type-1 segments, one type-2 segments and one type-3 curve. Type-1 segment $\tilde{\boldsymbol{x}}_1 - \tilde{\boldsymbol{x}}_2$ is associated with contact forces from the cell $I_1 \times I_2 \times O_3$ and the portion of segment $\tilde{\boldsymbol{x}}_2 - \tilde{\boldsymbol{x}}_3$ is associated with contact forces from the cell $O_1 \times I_2 \times I_3$. The type-2 SSI segment is associated with critical contact forces from the cell $I_1 \times S_2 \times S_3$. Finally, the type-3 curve is associated with critical contact forces from the cell $S_1 \times S_2 \times S_3$. Note that while computation of this boundary curve involve solution of complicated nonlinear equations, the boundary curves of types 1 and 2 are easily computed by solving simple linear programs. Thus, a reasonable

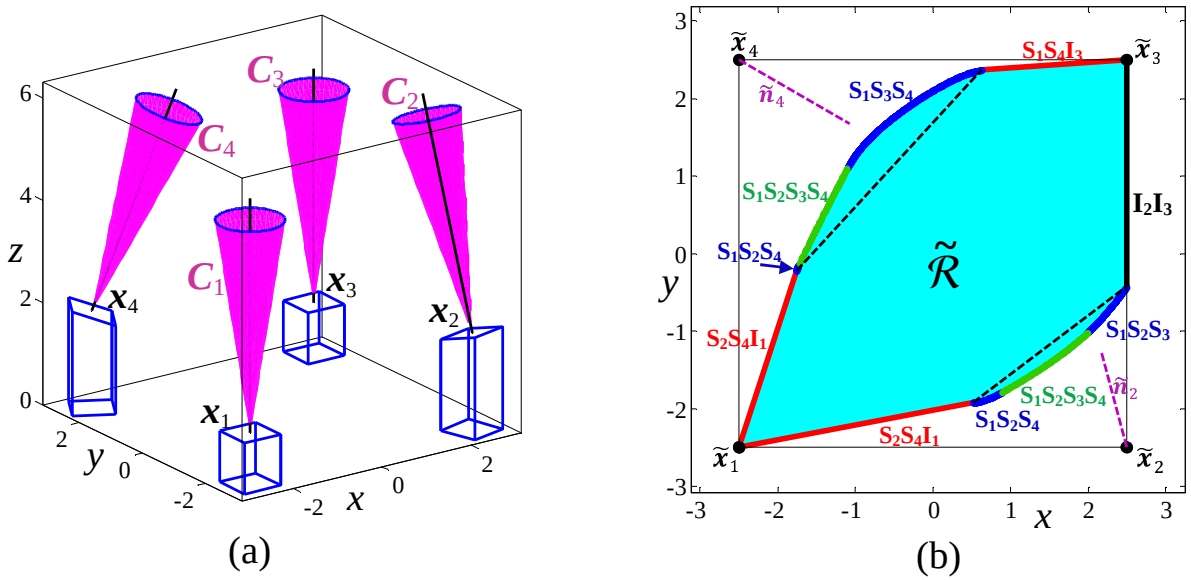

Figure 3: (a) The 4-contact arrangement in 3D. (b) Top view of the feasible equilibrium region $\widetilde{\mathcal{R}}$ and its four types of boundary curves.

and computationally cheap approximation of $\widetilde{\mathcal{R}}$ for this case could be obtained by replacing the nonlinear type 3 curve by a straight line segment connecting the endpoints p and q, as shown in a dashed line in the Figure. This gives a conservative polygonal region which is contained in $\widetilde{\mathcal{R}}$ and captures almost all its area (97%)..

Computational example - four contacts: the four contact locations are given by $r = 5/\sqrt{2}$, $\phi_i = \{-135°, -45°, 45°, 135°\}$ and $z_i = \{1, 1 + r/4, 1, 1 + r/4\}$. The contact normals' angles are given by $\alpha_i = \{0°, 15°, 0°, 60°\}$ and $\beta_i = \{0°, -15°, 0°, 20°\}$, and the friction coefficient at all contacts is 0.155. This contact arrangement, which is shown in Figure 3(a), can be verified as being tame, but contacts $\boldsymbol{x}_2$ and $\boldsymbol{x}_4$ are not quasi-flat. Figure 3(b) plots the equilibrium region $\widetilde{\mathcal{R}}$ for this contact arrangement in xy plane. The boundary of $\widetilde{\mathcal{R}}$ consists of a single II segment along the line $\tilde{\boldsymbol{x}}_1 - \tilde{\boldsymbol{x}}_2$, three SSI segments, four SSS curves and two $SSSS$ curves. The labels near each boundary piece give the indices of the contacts associated with S_i or I_i. One can see that using only II and SSI line segments and connecting their endpoints by straight lines (dashed segments in Figure 3(b)) again gives a conservative polygonal approximation of $\widetilde{\mathcal{R}}$ which reasonably captures the majority of its area (92%).

Computational example - five contacts: the five contact locations are given by $r = 5$, $\phi_i = \{-140°, -70°, 0°, 70°, 140°\}$ and $z_i = \{1 + r/4, 1 + r/4, 1, 1, 1\}$. The contact normals' angles are given by $\alpha_i = \{0°, -30°, 90°, 30°, 0°\}$ and $\beta_i = \{-20°, -30°, -40°, 30°, 20°\}$, and the friction coefficient at all contacts is 0.155. This contact arrangement, which is shown in Figure 4(a), can be verified as being tame, but none of the contacts are quasi-flat. Figure 4(b) plots the equilibrium region $\widetilde{\mathcal{R}}$ for this contact arrangement in xy plane. The boundary of $\widetilde{\mathcal{R}}$ consists of a single II segment along the line $\tilde{\boldsymbol{x}}_1 - \tilde{\boldsymbol{x}}_2$, two SSI segments, five SSS curves, four $SSSS$ curves and two $SSSSS$ curves. Note that the endpoints of the II segment are connected to very short pieces of SSS and $SSSS$ curves which are hardly visible in the figure. The labels near each boundary piece give the indices of the contacts associated with

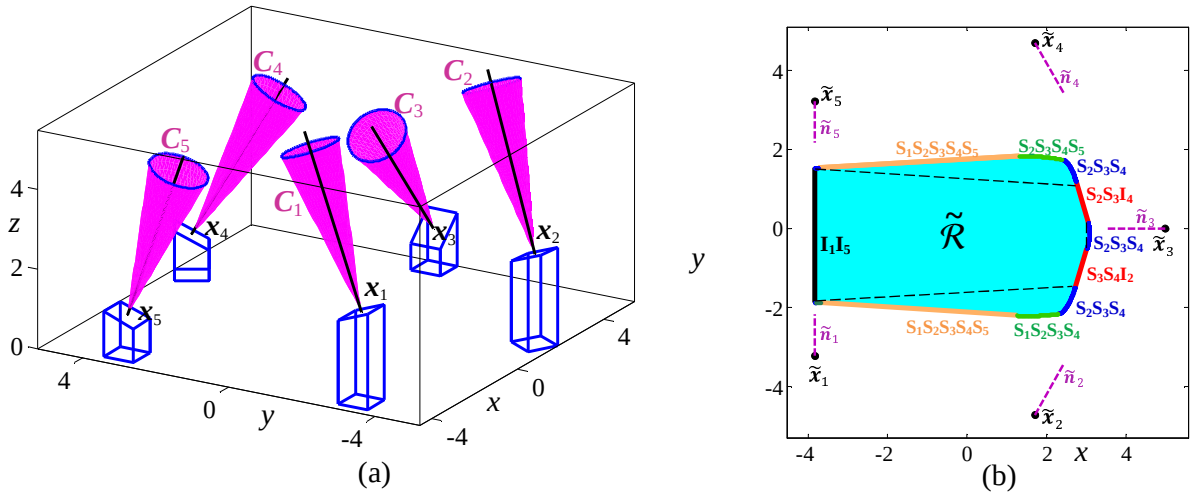

Figure 4: (a) The 5-contact arrangement in 3D. (b) Top view of the feasible equilibrium region $\widetilde{\mathcal{R}}$ and its five types of boundary curves.

it S_i or I_i. One can see that using only SSI line segments and connecting their endpoints by straight lines (dashed segments in Figure 4(b)) gives a conservative polygonal approximation of $\widetilde{\mathcal{R}}$ which captures most of its area (81%).

In order to validate Proposition 3.5, Figure 5(a) shows the five equilibrium regions $\widetilde{\mathcal{R}}_{ijkl}$ associated with four contacts for the same five-contact arrangement. One can see that the equilibrium region $\widetilde{\mathcal{R}}$ under five contacts (dashed curve) is indeed obtained as the convex hull of all four-contact regions. Finally, Figure 5(b) demonstrates the changes in the five-contact equilibrium region $\widetilde{\mathcal{R}}$ while the friction coefficient μ at all contacts is varied. Upon decreasing μ, the equilibrium region $\widetilde{\mathcal{R}}$ is monotonically shrinking. Starting with $\mu = 0.85$, all contacts are quasi-flat but the arrangement is still tame, hence $\widetilde{\mathcal{R}}$ is precisely the support polygon, as stated in Proposition 2.2. For $\mu = 0.6$ the contact $\boldsymbol{x}_3$ is no longer quasi-flat, hence $\tilde{\boldsymbol{x}}_3$ is no longer contained in $\widetilde{\mathcal{R}}$. For $\mu = 0.4$, only contacts $\boldsymbol{x}_1$ and $\boldsymbol{x}_5$ are still quasi-flat, so $\tilde{\boldsymbol{x}}_2, \tilde{\boldsymbol{x}}_3$ and $\tilde{\boldsymbol{x}}_4$ are no longer contained in $\widetilde{\mathcal{R}}$. For $\mu = 0.28$, all contacts are not quasi-flat but the boundary of $\widetilde{\mathcal{R}}$ still contains one type 1 boundary segment that lies on the line $\tilde{\boldsymbol{x}}_1 - \tilde{\boldsymbol{x}}_5$. $\mu = 0.155$ is the same value for which $\widetilde{\mathcal{R}}$ is computed in Figure 4(b). The equilibrium region $\widetilde{\mathcal{R}}$ is also shown for $\mu = 0.1$ and $\mu = 0.05$. For $\mu \to 0$ the equilibrium region shrinks to a single line segment, shown as the dashed line in the Figure. Note that the four-contact arrangement shown in Figure 3 is non-generic in the sense that the contacts $\boldsymbol{x}_1$ and $\boldsymbol{x}_2$ are flat i.e. $\boldsymbol{n}_1 = \boldsymbol{n}_2 = \boldsymbol{e}$. Thus, for frictionless contacts the equilibrium region $\widetilde{\mathcal{R}}$ degenerates to the line segment $\tilde{\boldsymbol{x}}_1 - \tilde{\boldsymbol{x}}_2$. This is in contrast to (8) that predicts that $\widetilde{\mathcal{R}}$ reduces to a single point for $\mu = 0$. Similarly, the three-contact arrangement in Figure 2 is also non-generic since $\boldsymbol{x}_1$ and $\boldsymbol{x}_2$ are flat. Thus, for frictionless contacts $\widetilde{\mathcal{R}}$ degenerates the line segment $\tilde{\boldsymbol{x}}_1 - \tilde{\boldsymbol{x}}_2$. This is in contrast to (8) that predicts that $\widetilde{\mathcal{R}}$ becomes empty for $\mu = 0$. An example of $\widetilde{\mathcal{R}}$ becoming empty for $n = 3$ contacts with $\mu \to 0$ has been shown in our previous paper.

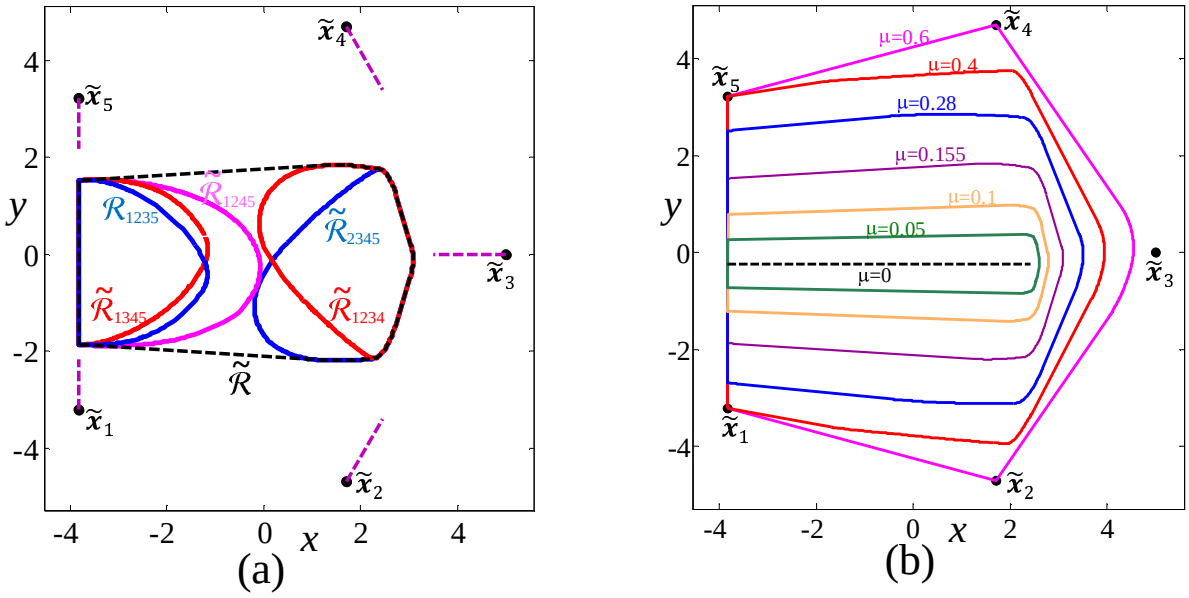

Figure 5: (a) The 5-contact arrangement in 3D. (b) Top view of the feasible equilibrium region $\widetilde{\mathcal{R}}$ and its five types of boundary curves.

5 Experimental results

This section describes experiments that measure the equilibrium region of a mutli-legged mechanism with a movable center of mass, which supported by a frictional terrain against gravity, as shown in Figure 6. The experiments have been conducted by the undergraduate students Erez Abitbul and Shai Tabib and the ME student Michael Dvorkin, at the laboratory of robot motion in the Technion. The objective of these experiments is to validate the analytical characterization of the equilibrium region $\widetilde{\mathcal{R}}$. The mechanism consists of a rigid aluminium ring with 36 holes around an outer circle of diameter 240mm. Three, four, or five extendible legs can be mounted to these holes, where each leg ends with a spherical footpad in order to maintain a point contact with its support. The legs are made of stainless steel, and are composed of inner and outer cylinders which can be assembled in three different lengths at 30mm increments. They can also be placed in any of the holes of the outer circle in order to control the relative positions of the contact points. Each footpad is supported by a stainless steel plate attached to a pair of V-shaped wooden plates whose relative angle can be varied continuously via lead screws, in order to control the direction of the contact normals. The mechanism's center of mass can be varied by sliding a heavy steel cylinder along linear guides which are rigidly connected to a base frame. The base frame can be mounted on top of the circular ring with screws that can be inserted in 24 different holes on the perimeter of an inner circle of diameter 189mm, allowing linear shift of the center of mass along different directions. The mass of each leg is 0.82 kg. The total mass of the circular ring, the rigidly attached base frame, and the linear guides is 6.17kg. The mass of the moving weight is 4.25 kg.

The coefficient of static friction between the footpads and supporting plates was measured in a preliminary experiment, in which a horizontal force was applied to the mechanism while its footpads are supported by horizontal plates. The horizontal force was applied by

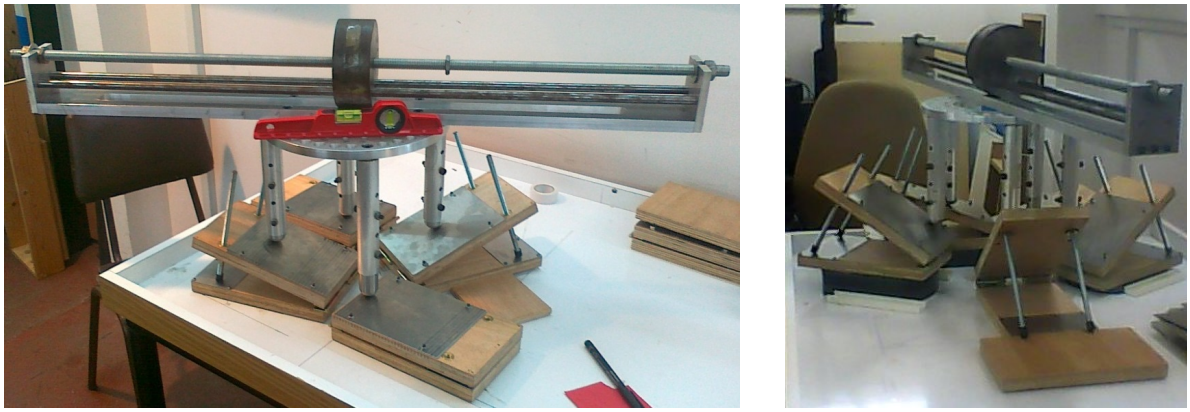

(a) (b)

Figure 6: Experimental setup of a the legged mechanism with (a) four legs, and (b) five legs.

hanging a variable weight on a string attached to the mechanism through a pulley. Measuring the critical weight that causes slippage of the footpads, the average coefficient of static friction has been determined as $\bar{\mu} = 0.155$ with a standard deviation of $\sigma = \pm 0.02$.

The process of measuring the boundary of $\widetilde{\mathcal{R}}$ is as follows. After assembling the chosen number of legs with desired lengths and relative positions, the mechanism is placed in static equilibrium on the supporting plates, whose positions and slopes are chosen according to the desired contact arrangement. The movable heavy cylinder is initially placed above the circular ring's center. Next, it is moved slowly outward along its guides in 1 mm increments, pausing after each increment to check that it maintains equilibrium while all contacts are stationary. This process continues until the mechanism's center of mass reaches the boundary of the equilibrium region, where a critical event of contact breakage or slippage is observed at one or more footpads. The critical center-of-mass position and the observed mode of non-static motion at the contacts are recorded, and the process is iterated several time in order to collect multiple measurements. Next, the base frame is mounted at a different orientation with respect to the ring, and the process is repeated. The orientations of the base frame eventually cover a full circle with 15° resolution, giving a discrete mapping of the boundary of $\widetilde{\mathcal{R}}$.

The experiments were conducted for three, four and five legs. The chosen contact arrangements were identical to the computational examples in section 4, as shown in Figures 2, 3 and 4, where the length units in the figures are scaled by a multiplying factor in order to match the actual size of the mechanism (i.e. $r = 240mm$). The experimental setup for four- and five-contact arragements are shown in Figures 6(a) and 6(b), respectively. The experimental results of the critical center-of-mass locations that compose the measured points on the boundary of the equilibrium region $\widetilde{\mathcal{R}}$ for the 3,4,5- contact arrangements are shown in Figures 7(a),(b),(c) respectively. The inner and outer equilibrium regions which are theoretically computed for friction coefficients of $\bar{\mu} - \sigma$ and $\bar{\mu} + \sigma$ are also overlayed in the figures, denoted by solid curves. Three different modes of motion were visually detected in the experiments: points marked by circles denote rolling over two contact points while all other contacts are separating. Points marked by squares denote rolling about one contact while the other contacts are either slipping or separating. Points marked by $'\times'$ denote simultaneous slippage at three or more contacts. A more elaborate distinction between all

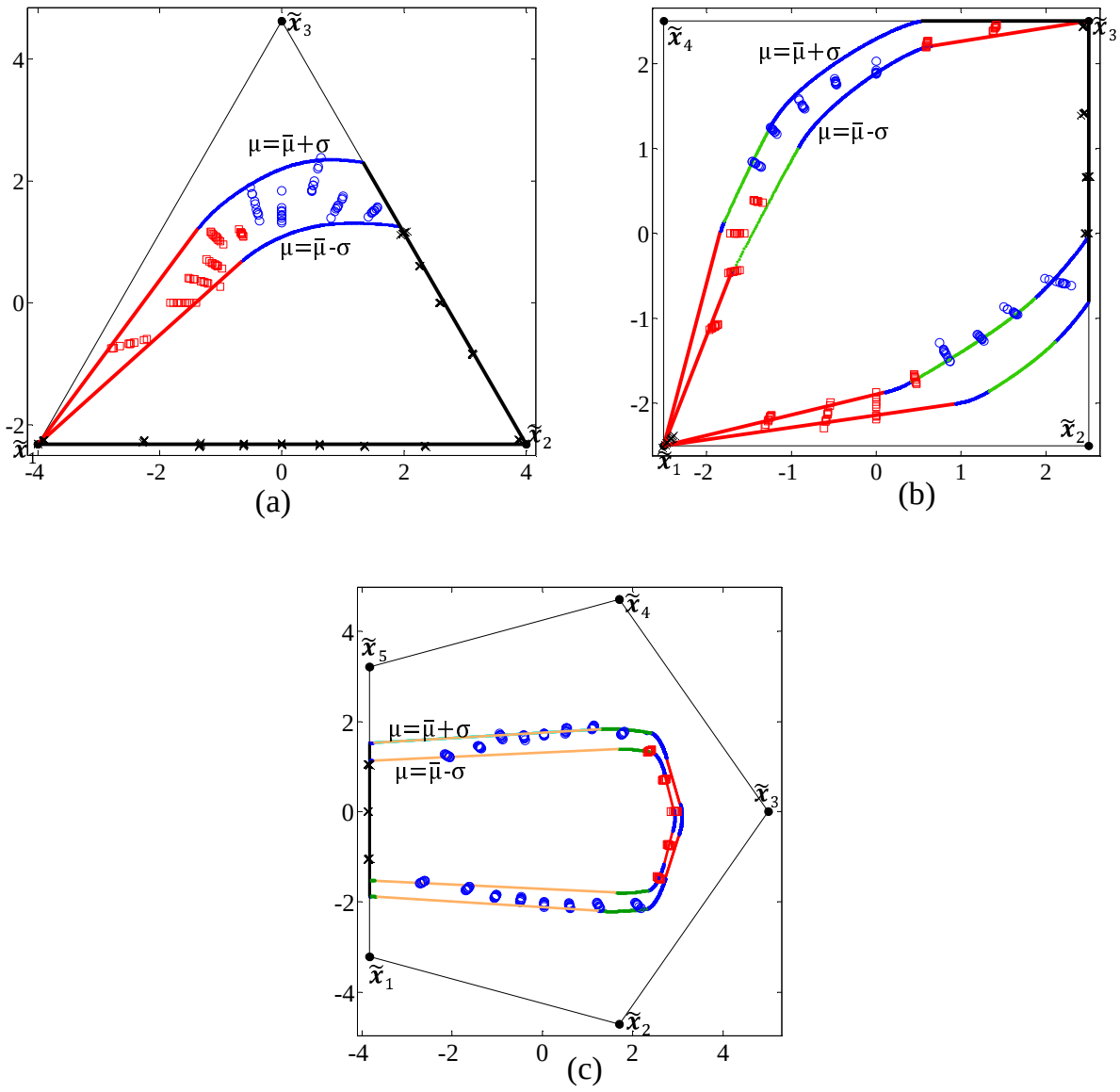

Figure 7: Experimental results of measured boundary of $\widetilde{\mathcal{R}}$ for (a) three legs, (b) four legs, and (c) five legs.

possible non-static contact modes by visual inspection only turned out to be impossible. The results show good agreement between the experimental measurements and the theoretical computation of the equilibrium region $\widetilde{\mathcal{R}}$ in all cases. In particular, it can be seen that the boundary points associated with two-contact rolling (marked by '$\times$' in the figures) are very accurate and display very small variations. This is because crossing these boundary points, which lie on segments of the support polygon, depends only on the geometry of the contact locations. On the other hand, measurement of boundary points of $\widetilde{\mathcal{R}}$ that involve slippage suffer from much larger variations. This is because their exact position depend on the friction coefficient, which is itself a sensitive quantity that is subject to variations. Nevertheless, most of the boundary points fall well within the range between the computed boundaries for $\mu = \bar{\mu} \pm \sigma$.

6 Polygonal approximation of the equilibrium region

This section complements the analytic results with a practical and efficient procedure for computing a polygonal approximation of the equilibrium region $\widetilde{\mathcal{R}}$. The procedure is based on approximating the frictional constraints (2) by linear inequalities and then using standard techniques for projecting a high-dimensional polyhedral region onto a two-dimensional plane in order to obtain inner and outer polygonal approximations for the boundary of $\widetilde{\mathcal{R}}$. It is slightly different from the adaptive algorithm presented by Bretl and Lall (2008), which solves a sequence of quadratic convex programming problems in order to compute inner and outer polygonal approximations and refine them iteratively. Our approach has recently been used in the work [Geva and Shapiro, 2013] for quasistatic motion planning of a quadruped robot on unstructured terrain.

The computation of $\widetilde{\mathcal{R}}$ can be represented as a problem of projecting a high-dimensional convex region onto a two-dimensional plane, which then naturally leads to a polygonal approximation of $\widetilde{\mathcal{R}}$, as follows. Recall that $\boldsymbol{f} = (\boldsymbol{f}_1, \boldsymbol{f}_2, \ldots \boldsymbol{f}_n) \in I\!R^{3n}$ denote the n contact forces. The static equilibrium equation (1) depends linearly on the contact forces, $\boldsymbol{f}$, as well as on the horizontal projection of the center-of-mass, $\tilde{\boldsymbol{x}}_c$. Hence it can be written in matrix form as $A\boldsymbol{f} = B\tilde{\boldsymbol{x}}_c$. The frictional inequality constraints $\boldsymbol{f}_i \in C_i$ specified in (2) for $i = 1 \ldots n$, along with the equilibrium condition (1) which adds six scalar linear equations, define a convex region, denoted $\mathcal{E}$, of dimension $(3n+2)-6 = 3n-4$ in the composite space of $(\boldsymbol{f}, \tilde{\boldsymbol{x}}_c)$. This region encodes all combinations of contact forces and center-of-mass locations which give a feasible solution of the static equilibrium condition subject to the frictional constraints. The *projection* of $\mathcal{E}$ onto the $\tilde{\boldsymbol{x}}_c$-plane is precisely the equilibrium region $\widetilde{\mathcal{R}}$. If the quadratic friction cones C_i in (2) are approximated by *polyhedral cones*, the inequalities $\boldsymbol{f}_i \in C_i$ become linear, and the region $\mathcal{E}$ becomes a convex polyhedron. The projection of $\mathcal{E}$ onto the $\tilde{\boldsymbol{x}}$-plane can be computed using standard projection algorithms such as Fourier-Motzkin method. Consider polyhedral cone C_i' with m facets inscribed in the friction cone C_i (Figure 8(a)). The inscribed polyhedral cone is given by m linear inequalities,

$$\begin{aligned} C_i' = \{\boldsymbol{f}_i : \ & (\sin((j+1)\beta) - \sin(j\beta))(\boldsymbol{f}_i \cdot \boldsymbol{s}_i) + (\cos(j\beta) - \cos((j+1)\beta))(\boldsymbol{f}_i \cdot \boldsymbol{t}_i) \\ & \leq \mu_i \sin\beta (\boldsymbol{f}_i \cdot \boldsymbol{n}_i) \ , \ j = 1 \ldots m\}, \end{aligned} \tag{29}$$

where $\beta = 2\pi/n$ and $\boldsymbol{s}_i, \boldsymbol{t}_i$ are two unit vectors such that $\{\boldsymbol{s}_i, \boldsymbol{t}_i, \boldsymbol{n}_i\}$ is a right-handed orthonormal frame at $\boldsymbol{x}_i$. The linear inequalities $\boldsymbol{f}_i \in C_i'$ for $i = 1 \ldots n$ along with the equilibrium

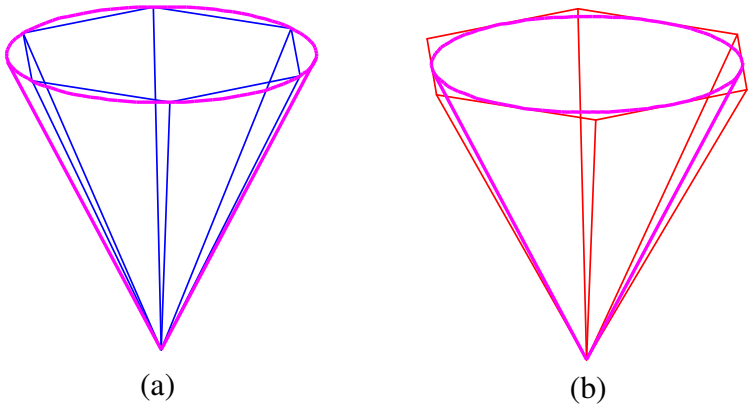

Figure 8: A six-facet approximation of the quadratic friction cone C_i by (a) an inscribed polyhedral cone C_i', and by (b) a circumscribing polyhedral cone C_i''.

equalities (1) define a polyhedral region $\mathcal{E}'$ in $(\boldsymbol{f}, \tilde{\boldsymbol{x}}_c)$-space. Moreover, since $C_i' \subset C_i$ for $i = 1 \ldots n$, this region satisfies $\mathcal{E}' \subset \mathcal{E}$. The projection of $\mathcal{E}'$ on the $\tilde{\boldsymbol{x}}_c$-plane gives a polygonal region $\widetilde{\mathcal{R}}' \subset \widetilde{\mathcal{R}}$ that serves as an *inner approximation* for $\widetilde{\mathcal{R}}$. This inner approximation can be made arbitrarily accurate by increasing the number of facets in C_i'. According to the analysis in [Ponce et al 1997] (which used the projection for computing 4-finger equilibrium grasps), the computation time of projection using Fourier-Motzkin method is $O(mnp)$, where p is the number of vertices in the resulting polygon $\widetilde{\mathcal{R}}'$. Similarly, one can define a second m-facet polyhedral cone, C_i'' , that *circumscribes* the quadratic friction cone C_i for $i = 1 \ldots n$ (Figure 8(b)), by simply replacing μ_i in the inequalities (29) by $\mu_i / \cos(\pi/m)$. Using C_i'' instead of C_i' results in a polyhedral region $\mathcal{E}'' \supset \mathcal{E}$ in $(\boldsymbol{f}, \tilde{\boldsymbol{x}}_c)$-space, whose projection on the $\tilde{\boldsymbol{x}}_c$-plane gives an *outer approximation* polygon, $\widetilde{\mathcal{R}}'' \subset \widetilde{\mathcal{R}}$.

Graphical example: Figure 9(a) shows an arrangement of five contacts and their physical friction cones in 3D. Figure 9(b) shows a top view (xy plane) of the contacts. The shaded region is the polygonal approximation of the equilibrium region, $\widetilde{\mathcal{R}}'$, obtained by projection of the polyhedral region $\mathcal{E}'$ where the friction cones are approximated by polyhedral cones C_i' with $m = 6$ facets. The outer approximation $\widetilde{\mathcal{R}}''$ appears in the dashed lines. Note that the polygons $\widetilde{\mathcal{R}}'$ and $\widetilde{\mathcal{R}}''$ are sensitive to the choice of the tangent vectors $\boldsymbol{s}_i$ and $\boldsymbol{t}_i$ in (29). Nevertheless, they give a tight bound to $\widetilde{\mathcal{R}}$, whose exact boundary must lie somewhere between the inner and outer polygons.

The procedure given above is a relatively efficient computational tool for approximating the equilibrium region $\widetilde{\mathcal{R}}$, where the accuracy can be controlled by choosing the number of facets m. The main limitation of this procedure is the lack of any physical intuition and geometric characterization on the boundary of $\widetilde{\mathcal{R}}$. For instance, Figure 9(b) indicates that the exact boundary of $\widetilde{\mathcal{R}}$ may consist of a combination of linear segments and nonlinear curves, without any apparent classification. The next section, which presents the exact computation of $\widetilde{\mathcal{R}}$, gives the classification into different types of boundary curves, along with their association to particular sets of constraints on the contact forces.

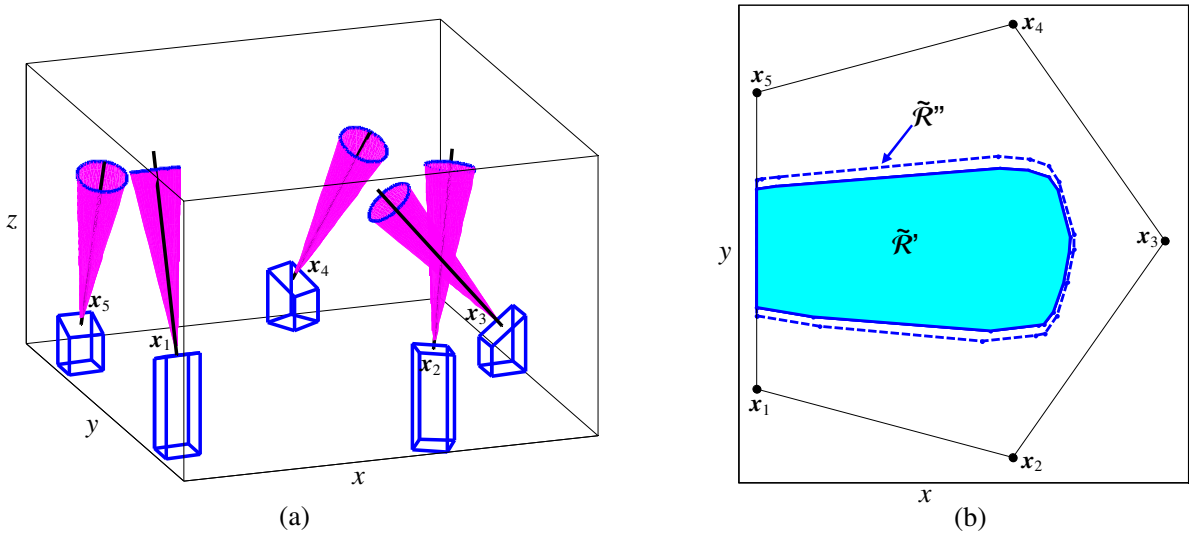

Figure 9: (a) A five-contact arrangement. (b) Top view with the inner and outer approximations $\widetilde{\mathcal{R}}'$ and $\widetilde{\mathcal{R}}''$ of the equilibrium region.